

Point-based Classification of Power Line Corridor Scene Using Random Forests

Heungsik B. Kim and Gunho Sohn

Abstract

The power line network, interconnecting power generation facilities and their end-users, is a critical infrastructure on which most of our socio-economic activities rely. As society becomes increasingly reliant on electricity, the rapid and effective monitoring of power line safety is critical. In particular, accurately knowing the current geometric and thermal status of power lines and identifying possible encroachments is the most important task in the power line risk management process. To facilitate this task, the correct identification of key objects comprising a power line corridor scene from remotely sensed data is the first important step. In recent years, airborne lidar has been successfully adopted as a cost-effective and accurate data source for mapping the power line corridors. However, in today's practice, the classification of power line objects using lidar data still relies on labor-intensive data manipulation, and its automation is urgently required. To address this problem, this paper proposes a point-based supervised classification method, which enables the identification of five utility corridor objects (wires, pylons, vegetation, buildings, and low objects) using airborne lidar data. A total of 21 features were investigated to illustrate the horizontal and vertical properties of power line objects. A non-parametric discriminative classifier, Random Forests model, was trained with refined features to label raw laser point clouds. The proposed classifier showed 91.04 percent sample-weighted and 90.07 percent class-weighted classification accuracy, which indicates it could be highly valuable for large-scale, rapid compilations of corridor maps. A sensitivity analysis of the proposed classifier suggested that when compared, training with class-balanced samples improves classification performance over training with unbalanced samples, particularly with corridor objects such as wires and pylons.

Introduction

Effective management of the power line network requires accurate power line mapping and monitoring. Power line mapping today is an on-site surveying process that urgently requires the improved capability to quickly and accurately detect, classify, and monitor objects within the corridor (Flood, 2011). These key corridor objects include terrain, vegetation, towers, power lines, buildings, roads and waterways. Traditionally such corridor scene analyses have relied on labor-intensive manual approaches that entail investigation of video footage captured on site. Recently, however, airborne lidar (Light Detection And Ranging) has attracted much attention for its potential to automate the complicated

data processing tasks required for corridor scene analysis (Ituen and Sohn, 2010). This is because airborne lidar can rapidly provide highly dense and accurate three-dimensional (3D) information of corridor objects without the use of ground control. Having such high quality 3D information will facilitate difficult photogrammetric computer vision tasks, such as feature extraction, feature grouping, and contextual analysis. Despite its potential, thus far not much research effort has been made employing airborne lidar data to explore classification methods of the corridor scenes. Hence, today's corridor mapping practice still remains an expensive physical process that is not suitable for the large-scale, rapid commercial compilation of corridor maps (Liang *et al.*, 2011). To address the indicated issue, this research investigated the potentials of a supervised learning classifier, specifically Random Forests, in the classification of corridor objects with airborne lidar data.

The classification is known as a computer vision process, which transforms remotely sensed data into information by properly assigning the class labels from a finite set of object classes to unknown observations. In the classification algorithms, a feature set measuring characteristic properties of the object classes for each observation provides basic input to differentiate one class from the others, or to group classes into clusters based on similar features (Guo *et al.*, 2012; Samadzadegan *et al.*, 2012). In lidar classification, the grid-based and point-based approaches are two distinct methods to extract the feature set. The grid-based approach considers 3D laser point cloud to be raster imagery, which is represented as a 2D array. In this method, the raw lidar point cloud is interpolated into a grid space, and each grid (pixel) contains representative information, such as height from the first return, number of returns, laser intensity, backscattering coefficient, width of reflected pulse, and so on. Lodha *et al.* (2007) used Gaussian Mixture Models to model training datasets obtained from grid lidar data, and applied the Expectation-Maximization (EM) algorithm to estimate supervised modeling parameters and posterior probabilities. A classification rule for specific objects was constructed from geometric and topological relations among regions resulting from segmentation over grid lidar data for detecting buildings (Forlani *et al.*, 2006); classifying forest types (Antonarakis *et al.*, 2008); detecting single trees (Zhang and Sohn, 2010; Lin *et al.*, 2011); and predicting single tree attributes (Yu *et al.*, 2011). Grid-based classification has often been used to fuse multiple laser echoes with multi-spectral information obtained from optical imagery for urban classification purposes (Guo *et al.*, 2011). A set of parameters extracted

Geomatics Engineering Program, Department of Earth and Space Science and Engineering, 312 Petrie Science & Engineering Building, York University, 4700 Keele Street, Toronto, Ontario M3J 1P3, Canada (hskim@yorku.ca).

from full-waveform lidar data was interpolated into an image grid to extract features for the classification of forest scenes using a Bayesian pair-wise classifier (Neuenschwander, 2009). The utilization of grid data provides the advantage of easy application of comprehensive low-level computer vision algorithms, such as region growing or other segmentation methods, without significant alterations, and the cost-effective management of the huge data volume in a lidar point cloud. However, grid-based classification implicitly assumes that a pixel represents only one class, although multiple scatters belonging to different classes are vertically distributed within the pixel. This may be a critical limitation to the classification of corridor scenes, where vertical overlaps exist between wire and terrain, vegetation and wire, wire and pylon, or vegetation and building.

In contrast to grid-based classification, the point-based method aims to extract a feature set and determine an object class for every single point. This requires a full investigation of individual laser points in 3D to label its corresponding object class. Rutzinger *et al.* (2008) proposed an object-based point analysis approach combining the segmentation and classification of full-waveform lidar data in 3D. Lu *et al.* (2009) classified individual lidar points into ground or non-ground by applying three levels of local features (point, segment, and disc) to conditional random fields (CRF). Niemeyer *et al.* (2011) also employed CRF to classify urban scenes; they created a graph where each node corresponds to a single point of lidar and each edge is represented as a link between a current point and its cylindrical neighborhood. Verma *et al.* (2006) used local planar properties extracted through principle component analysis (PCA) to detect building points. Carlberg *et al.* (2009) developed a series of binary classifiers, each of which can filter out a particular class from lidar points not labeled by preceding classifiers. This classification based on 3D features has been also applied to ground-based lidar using CRF (Lim *et al.*, 2009) or the Bayesian classifier (Lalonde *et al.*, 2006). The greatest benefit of the point-based approach is that multiple labels for each transmitted laser pulse can be determined according to the number of scatters and the material types interacting with the pulse, although the computational cost of such a plan would be expensive.

To date, only a few studies associated with power line classification or modeling have been reported. Jwa and Sohn (2012) combined a constrained non-linear least squares adjustment with the model selection process for estimating the parameters of catenary curve for reconstructing power line models from airborne lidar data. Melzer and Briese (2004) extracted power lines by applying iterative Hough transform (HT) to lidar data and grouping segmented line vectors through the Neural Gas Network. McLaughlin (2006) proposed a supervised knowledge-based classification method, where a learning model was established by applying Gaussian Mixture Model to eigenvalues computed from ellipsoid neighborhoods using lidar data. The above studies have reported success, but are limited to only few object classes (wire, vegetation, and terrain) and controlled environments where the scene contains a specific single type of power line that has little contact with vegetation. There are still increasing demands to advance classification algorithms to consider more diversified corridor instances including pylons, insulators and other power line attachments, and to make classifiers stable to variances within intra-object classes; for instance, a classification performance over power lines and pylons should not to be sensitive according to their voltage types.

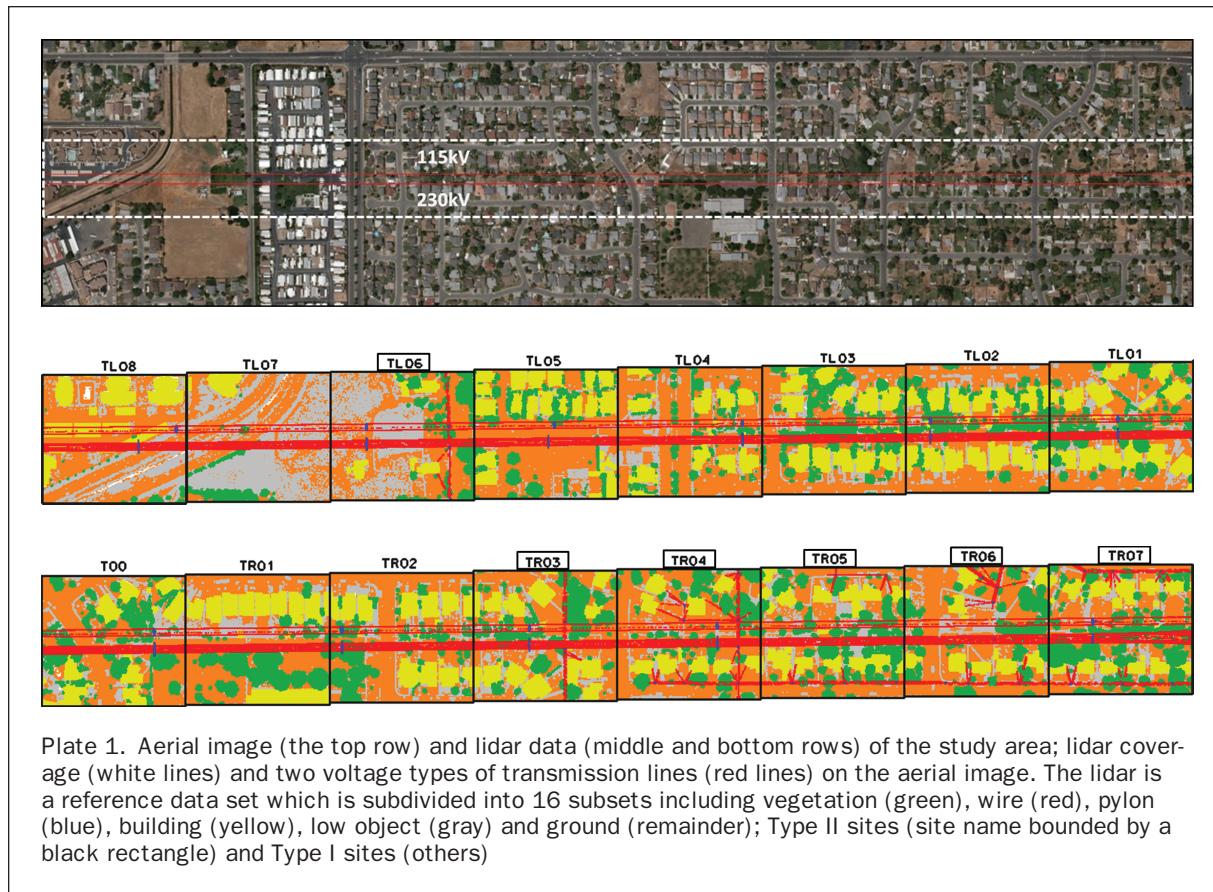
In this study, we propose a new point-based method to classify power line corridor scenes into five important classes (wire, pylons, buildings, vegetation and low objects) using airborne lidar data. A total of 21 features extracted from each

lidar point were introduced to distinguish the five classes. We adopted Random Forests as a supervised classifier to predict classes for unlabeled lidar points using a training sample and features. In the next section, we describe a test site used for our experiments, followed by introducing features that were used for power line classification and Random Forests. Experimental results are addressed with discussion, followed by our conclusions.

Study Area

Our study area is a power line corridor of 9.5 km (electrical substation to substation) in Sacramento, California (Plate 1). A RIEGL LMS-Q560 was mounted on a helicopter and scanned along the transmission corridor at an altitude of 300 m in August 2007. The lidar system acquired 24,929,992 points over the entire corridor with a point density of 25 to 30 points/m². An average laser footprint size was estimated to be 15 cm. For this research, we selected 10 spans (a span indicating the region between two consecutive pylons) that cover a total length of 1.9 km from the entire 65 spans in the corridor. A reference classification map (the second and third row in Plate 1) was produced using commercial software, called TerraScan, and in-house software by data processing expertise at GeoDigital International, Inc. (GDI). The selected spans were subdivided into 16 subsets called TL08 to TL01, T00, and TR01 to TR07, each of which has an equal size of 125 m × 100 m (length × width). We grouped all the subsets into two categories depending on the types of power lines and pylons contained in the scenes. Type I site is a subset that only has the transmission lines (TL08, TL07, TL05 to TL01, T00, TR01, and TR02), while Type II site contains both transmission and distribution lines (TL06, TR03, TR04, TR05, TR06, and TR07). Class-dependent site characteristics are described as follows:

- **Power lines:** The test corridor scene includes two different voltage types of transmission lines (115 kV and 230 kV) running parallel to each other, distribution lines (carrying below 110 kV) and pylons. The 230 kV transmission system is composed of six bundled cables and eight single cables, while the 115 kV system is composed of seven single cables. The transmission cables hang between 10 m to 40 m above ground. The distribution lines are present in some of the subsets and running parallel or perpendicular to the transmission lines. A tubal type and a steel lattice type of pylons support 230 kV and 115 kV transmission lines respectively, while the distribution lines are supported by simple and small pole type pylons, which height is less than 10 m. All the subsets have pylons except three sites, TL07, TL03, and TR01, which contain no pylon structures.
- **Building:** The power lines in the test scene run through a residential area where different types of buildings exist: mostly residential houses, commercial buildings, storage houses, and sun-shield roofs built over parking lots. Lidar points were captured by reflections from rooftops, but occasionally from building walls and chimneys. The overall height of the buildings is less than approximately 5 m. Most buildings are well detached from each other, but they make contact with trees at their edges on occasion.
- **Vegetation:** The test site contains a mixture of deciduous and coniferous trees, where deciduous trees are predominant. The coniferous trees are tall, narrow, and columnar resulting in a vertical structure similar to pylons. The tallest tree is 15 m high and the largest one has a 20 m diameter of tree crown.
- **Low object:** We define the low object class as a class that includes fences, vehicles, and grass. The fences are smaller than 2 m in height and are located between adjacent house gardens. Most of the vehicles are passenger cars, which have heights of 2 m or less. Large areas in TL08, TL07, and TL06 are covered by grass (Plate 1).
- **Ground:** In the corridor scene, the ground is the most predominant object. The ground surface is very flat except for a water region passing through the areas of TL07 and TL08 subsets (Plate 1).



Methodology

Feature Variables

We aim to develop a supervised classifier which can detect five key corridor object classes, that are vegetation, power line, pylon, building, and low object from a given utility corridor scene such as the one shown in Plate 1. In general, the five targeted corridor objects are visually distinguishable from each other. This is because the objects are differently formed with respect to surface characteristics that determine the degree of laser penetration, physical size and volume, surface roughness, structural patterns, and so forth. These discernible characteristics can be seen by examining a spatial distribution of lidar points, not only horizontally but also vertically. Thus, we investigated and computed 21 features for each lidar point by taking advantage of full 3D analysis (Table 1). The features are grouped into eight categories: *height*, *Hough Transformation*, *eigen-related*, *surface-related*, *convex hull*, *echo-related*, *density-related* and *vertical profile-related* feature. Depending on the feature group, a particular restricted space is used to collect neighboring points for each point: a sphere with radius r is used for *Hough transform*, *eigen-related*, *surface-related*, *echo-related* features and *point density*, while a vertical cylinder with radius r and height h is used for analyzing the property of vertical distribution of points such as *vertical profile-related* features. Here, the height h for the cylinder varies depending on the z range from neighboring points. Only *density ratio* is calculated by using both sphere and cylinder. In this article, the sphere and the cylinder for feature computation are denoted N_s and N_c , respectively, and the number of points captured by N_s and N_c are n_s and n_c . Figure 1 illustrates visualization maps

for the important features selected for a power line scene classification in this study.

Height from Ground Level

Height (HG) feature is an elevation measured from the terrain surface for each point above ground. The elevation of power lines is differently designed depending on the maximum voltage carried through them. In addition, the elevation can be considered a useful classification variable to differentiate residential buildings from the other classes such as pylon and vegetation. Similar to a method suggested by Lodha *et al.* (2007), we computed *HG* by measuring the vertical distance of each point from an underlying terrain surface model that is generated by applying a terrain filter proposed by Sohn and Dowman (2008) to lidar data.

Hough Transform

The geometry of a power line is formed as a catenary curve, but when it is projected onto a horizontal plane, the power line can also be represented with a set of line segments (Jwa and Sohn, 2012). Thus, analyzing linear properties for each point provides essential information for identifying power lines. The *Hough Transform (HT)* feature was designed to measure the likelihood that a lidar point belongs to linear structures such as power lines or pylon structures. We applied 2D Hough Transform (Hough, 1962) to 2D points obtained by projecting 3D points within N_s onto a horizontal plane. However, there are two limitations in applying the traditional Hough Transform to power line lidar data. The first is that 2D points corresponding to a cable are often not collinear due to systematic errors with airborne lidar. This may preclude the

TABLE 1. 3D AIRBORNE LIDAR FEATURES

Feature	Abbrev	Equation	Description
<i>Height</i>	HG	$e_i - e_g$	Height of each point (e_i , elevation) from ground (e_g)
<i>Hough Transformation</i>	HT	$\sum_{p=1}^{n_m} \left(v_p + \sum_{q=1}^8 v_{pq} \right) / n_m \times n_s$	Voting to measure linear-likeness in Hough space where n_m is the number of the local peaks considered for the voting procedure, v_p is the voting count for each peak, and v_{pq} is the voting counts in the cells adjacent to each peak.
<i>Eigen</i>	SP	λ_3 / λ_1	<i>Eigenvalues</i> , $\lambda_1 > \lambda_2 > \lambda_3$, a measure of spherical-likeness
	LN	$(\lambda_1 - \lambda_2) / \lambda_1$	A measure of linear-likeness
	PL	$(\lambda_2 - \lambda_3) / \lambda_1$	A measure of planar-likeness
	AN	$(\lambda_1 - \lambda_3) / \lambda_1$	Asymmetric volume property of an object
<i>Surface</i>	PS	$\Delta\theta$	Angle difference between plane normal vector and z-axis
	OD	-	Root mean square of perpendicular distances from each point to plane
	VD	-	Root mean square of vertical distances from z point values to corresponding z value on plane
	SN	$\sum_{i=1}^{n_T} (\Delta\theta_i - \bar{\Delta\theta})^2 / n_T$	Variance of <i>Plane Slope</i> ($\Delta\theta$) of n_T triangles in a mesh surface
<i>Convex Hull</i>	PA	$A / (\pi \cdot r^2)$	Bounding area of points projected on a horizontal plane (A)
	BV	$V / (4\pi \cdot r^3 / 3)$	Bounding volume of 3D convex-hull (V)
<i>Echo</i>	VE	$(n_{fr} + n_{ir}) / n_s$	Proportion of first (n_{fr}) and intermediate (n_{ir}) returns to all points (n_s)
	BE	n_{sr} / n_s	Proportion of single (n_{sr}) returns
	TE	$(n_{sr} + n_{lr}) / n_s$	Proportion of single (n_{sr}) and last (n_{lr}) returns
	PE	n_{fr} / n_s	Proportion of first (n_{fr}) returns
<i>Density</i>	PD	$3 \cdot n_s / 4\pi r^3$	Density of points within a sphere
	DR	$3 \cdot n_s / (4\pi r^2) \approx n_s / n_r$	Ration of point densities in a sphere and in a circle projected on a horizontal plane.
<i>Vertical profile</i>	OS	-	# of occupied bins
	COS	-	Maximum # of sequentially occupied bins
	CFS	-	Maximum # of sequentially empty bins

points from being mapped into a certain cell in the Hough grid, but they may be mapped into close cells to the cell with the highest count. The second is that N_s could contain multiple cables, such as bundled conductors, which will produce n_m peaks ($n_m > 1$). Therefore, for HT we take into account n_m peaks (v_p is a vote count for each peak) and v_{pq} , the vote count in the cells adjacent to each peak in the grid. With this method, HT measures the total number of supports through the presence of linear features. In Table 1, the HT feature is computed by calculating all of the votes normalized by n_m and n_s , where n_m is heuristically determined using the site knowledge (assumed $n_m = 4$ in this study).

Eigenvalue-related Features

Analyzing eigenvectors and eigenvalues often provides useful information to classify objects in an image. To classify an urban scene using lidar data, Chehata *et al.* (2009) defined four eigenvalue-related features including *Sphericity* (SP), *Linearity* (LN), *Planarity* (PL), and *Anisotropy* (AN). In this study, three eigenvectors are computed using all lidar points in N_s centered at one point. According to Chehata *et al.* (2009), SP is a measure of how spherical (round) an object is, while LN and PL are measures of how linear or planar an object is respectively; AN is a measure of the directional anisotropic property of an underlying object. The equations of the eigenvalue-related features are described in Table 1. SP is useful

for differentiating vegetations from the other objects, while the values of LN and PL would be higher for power lines and buildings, respectively. AN helps to differentiate power lines and buildings from vegetation by showing an inequality of the scalars with three eigenvectors.

Surface-related Features

We extracted surface-related features that are relevant attributes to characterize planar objects such as building rooftops. For each point, a plane surface was approximated over a set of points captured by N_s . Then, *Plane Slope* (PS), *Orthogonal Distance* (OD), and *Vertical Distance* (VD) were computed on the basis of the estimated plane. PS is the angular difference between the surface normal to the plane and the z-axis. OD and VD both represent surface residual, but they are different in the method of residual measurement, the approaches being orthogonal and vertical residual, respectively. The last feature, called *Homogeneity of Surface Normal* (SN), is defined as a measure of surface roughness of an object with respect to the similarity between normal vectors of n_T triangles approximating the surface of the object. A 3D triangular mesh surface is created from points in N_s . PS would be expected to show regular slope values over buildings, while arbitrary slopes over vegetation. Two surface roughness measures (OD and VD) are useful features in distinction between buildings with smooth surfaces and vegetation that shows high surface roughness

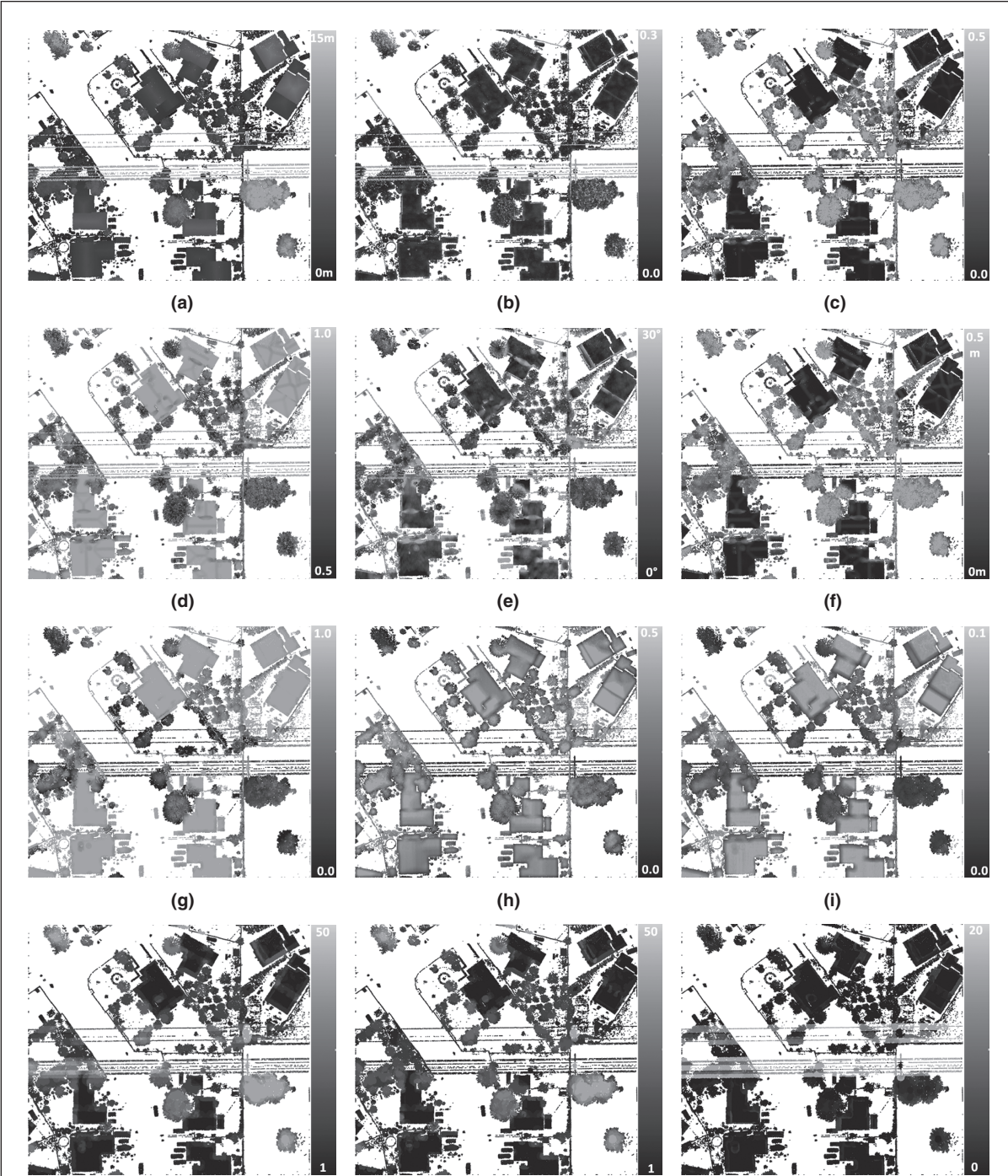


Figure 1. Visualization of important feature images: (a) HG, (b) HT, (c) SP, (d) AN, (e) SN, (f) OD, (g) PH, (h) PD, (i) DR, (j) OS, (k) cos, and (l) CFS.

(Rutzinger *et al.*, 2008). However, **OD** and **VD** might not be suitable for measuring the surface roughness of a region where multiple planes intersect. In this case, **SN** is able to overcome this difficulty by measuring a local transit between the normal vectors of neighboring surfaces at relatively finer scale compared to the one for computing **OD** and **VD**.

Convex Hull-related Features

Convex hull-related features are examined to measure the volumetric property of an object of interest captured by N_s for

each point. Two features, **Projection Area (PA)** and **Bounding Volume (BV)** are defined similar to the work by Yu *et al.* (2011). **PA** is computed by applying a 2D convex hull algorithm to 2D points produced by a horizontal projection of the points in N_s , and then normalizing the area of the convex polygon to the area of a circle with radius r of N_s . **BV** is computed by applying a 3D convex-hull algorithm directly to 3D points in N_s and then normalizing the volume of the generated polyhedron to the volume of N_s . In general, vegetation will show high values in both **PA** and **BA** as it usually has a large volume,

while a building will have high **PA** and low **BV** values, as its rooftop occupies a large space in 2D, but it is small in depth. The power lines will show small values in both **PA** and **BA** as they usually occupy small spaces in both horizontal and vertical space. However, a pylon might be difficult to characterize with respect to **PA** and **BA** as it has different shapes; pole-type towers would show low values in both **PA** and **BA**, while steel-frame towers would show high values.

Echo-related Features

Lidar is able to capture multiple echoes (returns) from a single laser shot. According to the number and the order of returns, the echo is classified into single return, first return, intermediate return, or last return. This echo information is a well-used feature to distinguish penetrable objects (e.g., tree and shrub) from rigid objects (e.g., building rooftops and terrain). For instance, most echoes from vegetation (*Vegetation Echo, VE*) are likely to be first returns or intermediate returns (Rutzinger *et al.*, 2008). Single returns are predominant for building (*Building Echo, BE*), while both single and last returns are recorded for terrain (*Terrain Echo, TE*). Thus, the echo-related features for vegetation, building and terrain were designed by considering the aforementioned returning patterns. In this study, another feature (*Power line Echo, PE*) is introduced for classifying power lines that usually present first echoes from power cables and other echoes from underlying features due to the relatively larger footprint of a laser beam compared to the diameter of a power cable. Depending on the pylon type, the echo patterns vary; the echo pattern of a steel-framed pylon would be similar to that of vegetation, while a pole-typed pylon may show a similar echo pattern to a building. Table 1 summarizes the echo-related features, where n_{sr} , n_{fr} , n_{ir} , and n_{lr} are respectively the number of points corresponding to single, first, intermediate, and last echoes captured within N_s .

Density-related Features

The number of lidar points reflected from a unit surface area varies depending on the surface characteristic illuminated by the laser beam, which determines the degree of laser penetration of the surface. We investigated two density-based features, *Point Density (PD)* and *Density Ratio (DR)* as classification features. **PD** is defined as the number of points within N_s divided by the volume of a sphere for N_s . In general, a higher **PD** would be usually obtained over a solid surface (e.g., building) than over a penetrable object (e.g., vegetation or power line). Also, a **PD** obtained over vegetation would be higher than one from power lines as vegetation usually has more scatters contained within a fixed volume size. We adopt **DR** as an additional feature that was initially proposed by Rutzinger *et al.* (2008) for identifying vegetation using airborne lidar data. **DR** is computed as a ratio of **PD** in 3D, which is the point density in a sphere, to **PD** in 2D, which is a point density in a circle created by projecting the sphere onto a horizontal plane. **DR** is approximated as a ratio between point counts (n_s and n_c in Table 1) within N_s and N_c . As can be seen in Figure 1h and 1i, **PD** shows different values over rooftops as it is affected by relative view angles between a laser scanner and the target's surface normal. However, **DR** is relatively less affected by this factor.

Vertical Profile-related Features

Recently, there has been a rising interest in detecting vertical objects (tree trunks, traffic lights, lamp posts, etc.) from ground-based ranging imagery (Lehtomäki *et al.*, 2010; Kim and Medioni, 2011; Rabbani and van den Heuvel, 2005). Although the proposed methods successfully demonstrated their performance, there are some limitations that hinder

their direct application to detecting vertical objects in a corridor scene. This is partly due to the diversity in shapes of vertical objects from simple (pole-typed) to complex (steel-framed) pylon and also partly due to a relatively insufficient point density compared to ground-based lidar data. Thus, we devised new features, called vertical profile-related features, to characterize the property of vertical distribution of lidar points reflected from corridor objects. A cylinder with radius r and height h is created by N_c of a point. Then, the cylinder is vertically divided by a fixed incremental height, Δh that produces a number of cylinder segments. A cylinder segment is marked as an occupied segment, called on-segment, if it contains more points than a pre-specified threshold; otherwise, it is marked as an off-segment. The vertical profile-related features are computed by measuring three different counts: (a) the maximum number of on-segments that are continuously connected, called the *Continuous On-Segment (cos)*; (b) the maximum number of off-segments that are continuously connected, called the *Continuous Off-Segment (cfs)*; and (c) the total number of *On-Segments (os)*. Vegetation and pylons would be expected to show high values in **cos**, while demonstrating low **cfs** values. A vertically discontinuous object such as a power line and a building would show high values in **cfs**, while displaying low values in **cos**. The count of *On-Segment (os)* is also taken into account in characterizing the properties of a vertically structure object such as pylon.

Random Forests

Random Forests have been successfully studied for land-cover mapping from satellite imagery (Na *et al.*, 2010; Rodriguez-Galiano *et al.*, 2012; Waske and Braun, 2009), for the prediction of tree inventory (Coulston *et al.*, 2012; Yu *et al.*, 2011) from lidar, and for the classification of urban scenes from lidar and color images (Guo *et al.*, 2011). Moreover, some of the studies have reported that Random Forests yield better classification results than single classifiers (Na *et al.*, 2010; Waske and Braun, 2009).

Random Forests (Breiman, 2001) is a state-of-the-art ensemble learner accommodating multiple trees trained with corresponding samples. Each sample is randomly drawn from training data with replacement. While training, about one-third of a drawn sample is excluded, called "out-of-bag" or OOB, and the remaining two-thirds, called "in bag", generates a single tree. For the growth of a tree, each descendant node (or subsample) is split from a parent node using a random subset of input variables (i.e., features), which minimizes the class impurity within the descendant nodes (Sutton, 2005). The "out-of-bag" is an independent test set used for internally evaluating a tree generated by the "in-bag." The importance of each feature, or the contribution of each to overall classification performance, is measured by the "out-of-bag" test using the permutation accuracy (Breiman, 2001; Guo *et al.*, 2011). An optimal feature subset is normally determined based on the feature importance and used for learning a Random Forests classifier. The multiple trained trees are applied to a test set to be classified. The class label for each instance in the test set is decided by the majority vote over all the trees. Two parameters are required to run Random Forests: T , the number of populated trees and F , the number of used features for each node split.

Balanced Learning

Training classification models with an unbalanced sample containing unequal numbers of instances in classes is a potential problem in practical classification (Chen *et al.*, 2004). Using unbalanced data, most supervised classification algorithms tend to learn toward correct classification of the majority classes, rather than paying special attention to the minority classes. An airborne lidar system for power utility

management typically collects laser point clouds along a main center line of power lines and covers tens of meters of a buffer area (approximately 50 m in our data) from the center line. Coverage for wire (4.26 percent), pylon (0.81 percent) and low object (15.06 percent) in the buffer area is considerably smaller compared to that of other classes (vegetation, 46.46 percent, and building 33.41 percent). Here, a number in each bracket stands for the class proportion of the test site T00 in Plate 1. Such unbalanced data also affects feature selection as the feature importance is estimated by measuring overall classification errors using samples drawn from the unbalanced training data. Consequently, features associated with the majority classes will be more important in their contributions to classification results. To solve this issue of imbalance, we balanced our training data using a combination of under-sampling majority classes and over-sampling minority classes which is introduced by Chawla *et al.* (2002).

Accuracy Assessment

Similar to a method suggested by Lodha *et al.* (2007), we evaluate the performance of classifiers using two types of accuracies by comparing classification results and reference data: sample-weighted and class-weighted accuracy. The sample-weighted accuracy is the percentage of correctly classified points to entire numbers of points, while the class-weighted accuracy for a class is the percentage of points correctly labeled as the class to points having the same class label in the reference data. The sample-weighted accuracy indicates the overall classification performance regardless of the degree of predominance of each class in the entire scene. However, the class-weighted accuracy represents the classification performance of a classifier for each class. A good classifier satisfies high accuracy in both measures.

Experimental Results and Discussion

We conducted a classification performance analysis of the Random Forests trained with the proposed features using a corridor scene (16 subsets) shown in Plate 1. For extracting features shown in Table 1, two parameters of r and Δh were fixed as 1.5 m and 0.75 m, respectively, to determine the size of neighboring systems of sphere (N_s) and cylinder (N_c). To train the Random Forests, the number of trees T was set to 60, while the number of features F was differently set to 5 for 21 feature case and 3 for 7 feature case. We empirically set those parameters through trial-and-error experiments to make an optimal balance between classification accuracy and computational cost. Please note that we utilize the site knowledge of minimum height separation between transmission lines of 1.5 m to determine Δh (half of the minimum height), while we follow typical practice in modeling Random Forests to determine F subjectively with given M by rounding the numeric values of $\log_2(M) + 1$.

In the first two sections, a comparative performance analysis of balanced and unbalanced training samples, and the feature refinement process are presented. Then we discuss the sensitivity analysis of the proposed classifier to training samples and scene contents. Finally, a comparative analysis of the performance of the proposed point-based classifier to the grid-based one is examined.

Balanced versus Unbalanced Learning

We generated a Random Forest with a balanced training sample and compared its performance to the one obtained with an unbalanced sample. The training sample was arbitrarily chosen as T00 in Plate 1. The balanced training sample was produced as previously discussed from the original T00 (unbalanced). Figure 2 presents the classification accuracies per class for two classifiers modeled with the balanced T00 and the unbalanced T00. The results showed that balanced learning produced more accurate classification results (97.95 percent) than unbalanced learning (96.62 percent). We also found that balanced learning is more effective in avoiding biases in classification due to unequal class distribution in the unbalanced sample. In the results, balanced learning produced 4.4 percent higher accuracy over the minority classes (i.e., wire, pylon and low object) compared to unbalanced learning. The reduction of the classification errors in such key objects is critical for conducting the power line safety analysis. Therefore, all the trainings henceforth were performed with balanced training samples.

Feature Refinement

The feature refinement process aims to reduce the excessive feature dimensionality by selecting the most suitable features containing relevant information to the targeted classes and linearly combining those features. We conducted the feature selection by computing the feature importance following the method proposed by Guo *et al.* (2011). Figure 3 shows the computed feature importance for classification results produced by learning the balanced T00: the higher the value, the more important the feature. We categorized each feature into one of five feature groups (vegetation, wire, pylon, building, and common) according to its relevance to the designated feature group. Note that we did not specify the features for low object class as it is comprised of various objects, and thus the generalization of its characteristics is difficult. Instead, the low objects were mostly characterized by HG (height from the ground), which is categorized in the common feature group. To find important features, we selected the features whose importance shows a higher value than the threshold of 5 percent, which value was empirically set. Among the selected features, a final feature set (f_{12}) was determined by selecting the two most important features from each class and four as common features (black-boxed features in Figure 3). The same

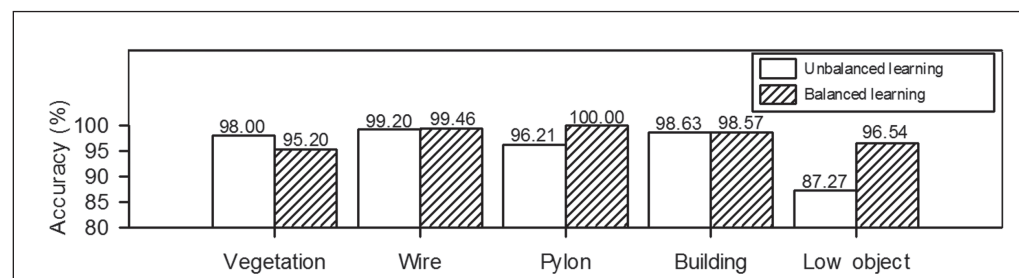


Figure 2. Class-weighted accuracies of unbalanced and balanced learning for site T00.

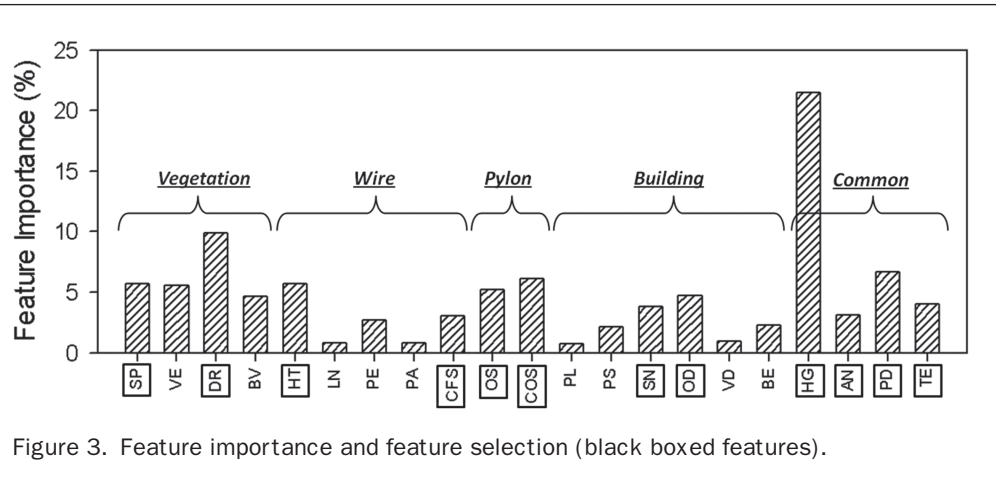


Figure 3. Feature importance and feature selection (black boxed features).

numbers of features were selected for each class in order to avoid biased contributions of features to specific classes.

Figure 4a shows a correlation of each pair of features in the selected feature set (f_{12}). As shown in the figure, several features including SP-AN and DR-PD are highly correlated with each other. We employed PCA (Principal Component Analysis) to reduce such connections between the feature pairs. We chose first K principle components maintaining 95 percent of information ($K = 7$ is determined as shown in Figure 4b). Finally, seven dimensional features (f_7) were produced. The same procedure for the feature selection was applied to all the test sites, so that they have an identical feature set f_7 .

Sensitivity Analysis to Training Sites

The classification results will be produced differently even over the same scene if the classifier is trained with different sample. To investigate its sensitivity to the training samples, we produced four different classifiers (C_{T00} , C_{T02} , C_{TL06} , and C_{TR03}). Each classifier was modeled using Random Forests with the balanced T00, TR02, TL06, and TR03, respectively, and with the refined feature subsets (f_7). We selected T00 and TR02 representative of Type I sites, which contain only transmission lines, while TL06 and TR03 represented Type II sites, containing both distribution and transmission lines.

Table 2 presents class-weighted and sample-weighted accuracies, which were computed by Type I (C_{T00} and C_{T02}) and Type II classifiers (C_{TL06} and C_{TR03}). Table 2 suggests that selecting training sites affect the class-weighted classification accuracy. Type II classifiers yielded better overall class-weighted accuracies than Type I classifiers, while the opposite results can be observed in sample-weighted accuracy. In particular, compared with Type I classifiers, Type II classifiers resulted in more accurate classification for the wire, pylon, and low object classes. An ideal classifier is able to produce high classification performance in both sample-weighted and class-weighted accuracies. In this regard, C_{TR03} yielded the highest efficiency in both accuracies. Moreover, corridor scenes often contain different types of power lines and pylons. It is critical to correctly classify diverse objects with intra-class variations for power line mapping. C_{TR03} (Type II) showed relatively higher class-weighted accuracy in both object classes. This suggests that selecting a training site containing many different objects existing over test sites is important for training an optimal classification model.

Classification Performance Analysis

We selected C_{TR03} as the optimal classifier, demonstrating the leading classification performance. Plate 2 shows a

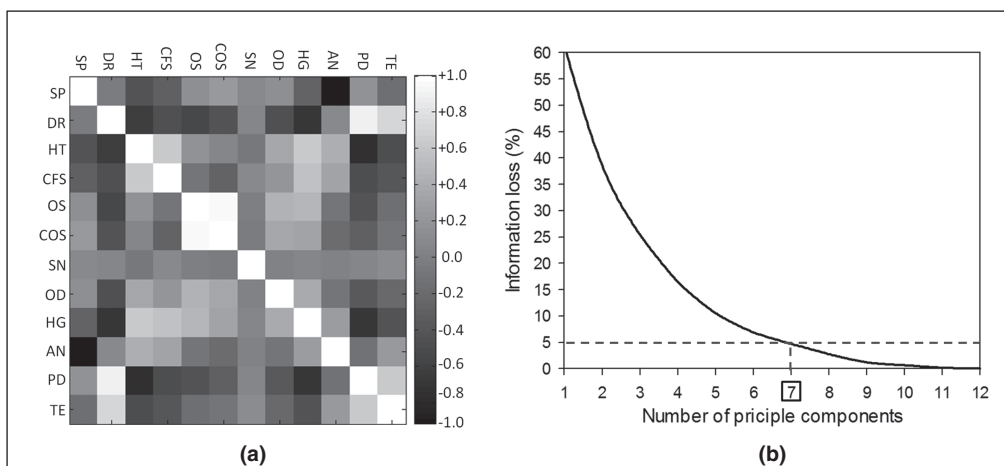


Figure 4. Feature generation using PCA (Principle Component Analysis): (a) a correlation of each pair of features (12) in the selected feature set, and (b) the first K principle components maintaining 95 percent of the information: $K = 7$.

TABLE 2. CLASS-WEIGHTED AND SAMPLE-WEIGHTED ACCURACIES OF TYPE I AND TYPE II CLASSIFIER

Classifier	Class-weighted accuracy (%)						Sample-weighted Accuracy (%)	
	Vegetation	Wire	Pylon	Building	Low object	Average		
Type I classifier	C_{T00}	91.79	87.92	86.79	94.05	83.56	88.82	91.11
	C_{TR02}	91.56	90.92	73.18	94.90	86.97	87.51	91.92
Type II classifier	C_{TL06}	88.58	93.44	88.71	90.59	87.32	89.73	89.34
	C_{TR03}	90.20	93.10	85.49	92.92	88.64	90.07	91.04

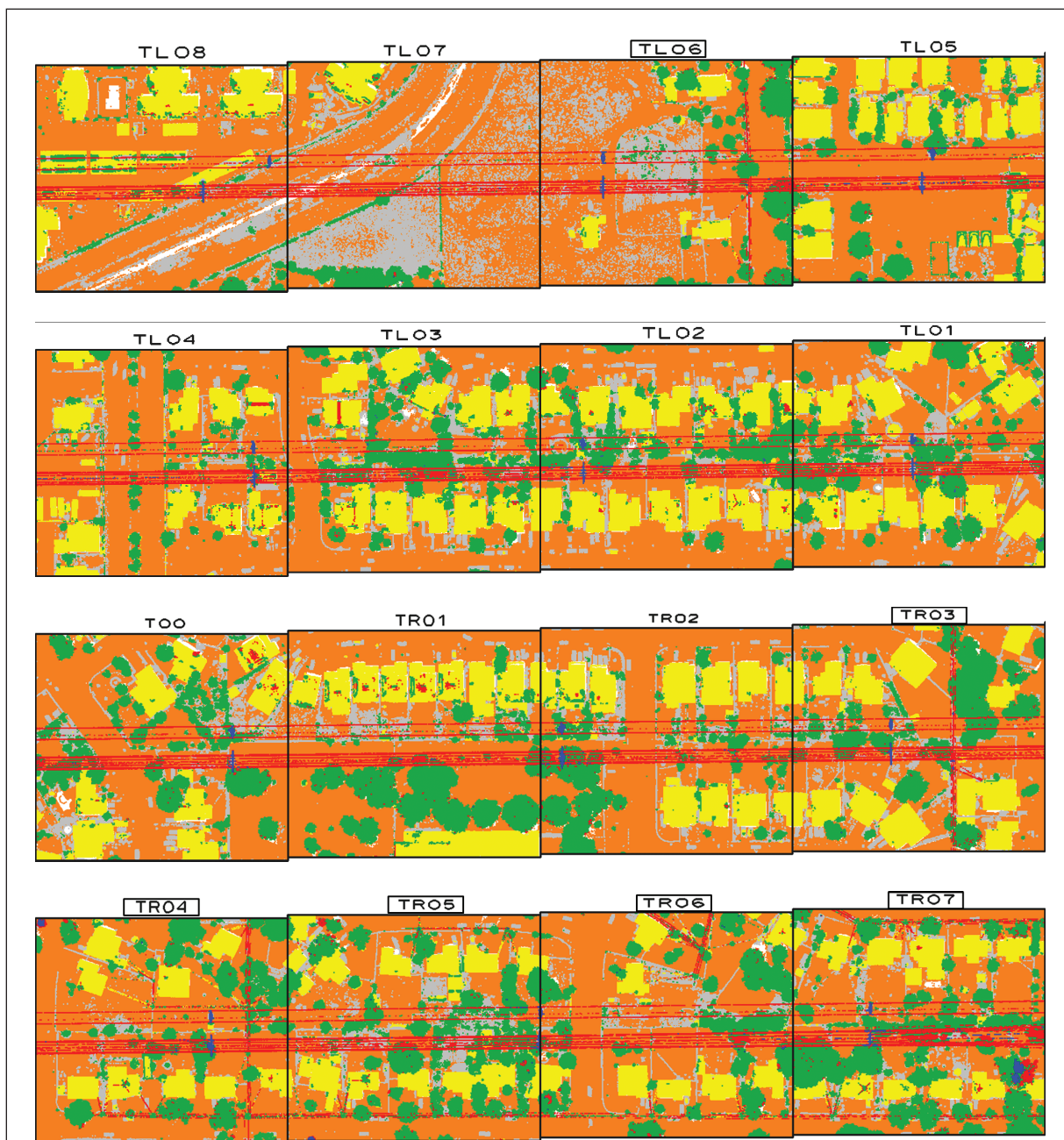


Plate 2. Classification map for all sites: vegetation (green), wire (red), pylon (blue), building (yellow), low object (gray) and ground (remainder); Type II sites (site name bounded by a black rectangle) and Type I sites (others)

classification map produced by applying C_{TR03} to all 16 sites. Figure 5 provides the class-weighted accuracy for each site, and Table 3 presents a confusion matrix that suggests commission and omission errors per class produced by C_{TR03} . As shown in Figure 5, the proposed classification method achieved the class-weighted accuracy in the range of 84.40 percent to 98.48 percent for the classes. Its average accuracy was estimated at 90.78 percent, with 3.84 percent standard deviation across the sites. For all the sites, the wire class shows the highest classification accuracy of 93.10 percent and similar accuracies can be found for the building class

(92.92 percent) and the vegetation class (90.20 percent). The pylon and low object classes record lower accuracies of 90 percent. Figure 6 shows classification maps over TR02 and TR06. TR02 (Type I site) obtained the highest class-weighted accuracy of 94.31 percent excluding the training site (TR03), while TR06 (Type II site) reported the most inferior class-weighted accuracy of 83.61 percent.

In Type II sites, the class-weighted accuracies for the wire and pylon classes are relatively lower than those in Type I sites due to the misclassification of distribution lines and small pylons into vegetation. We believe that such an

TABLE 3. CONFUSION MATRIX ACROSS ALL SITES ($F = 3, T = 60$)

		Predicted					Omission error (%)
Class		Vegetation	Wire	Pylon	Building	Low object	
Actual	Vegetation	1,175,449	9,204	2,171	17,323	99,042	9.80
	Wire	7,154	131,628	1,412	825	372	6.90
	Pylon	944	1,705	16,386	26	107	14.51
	Building	36,767	2,594	71	1,005,384	37,154	7.08
	Low object	30,336	338	50	22,374	414,476	11.36
	Commission error (%)	6.01	9.51	18.44	3.88	24.80	

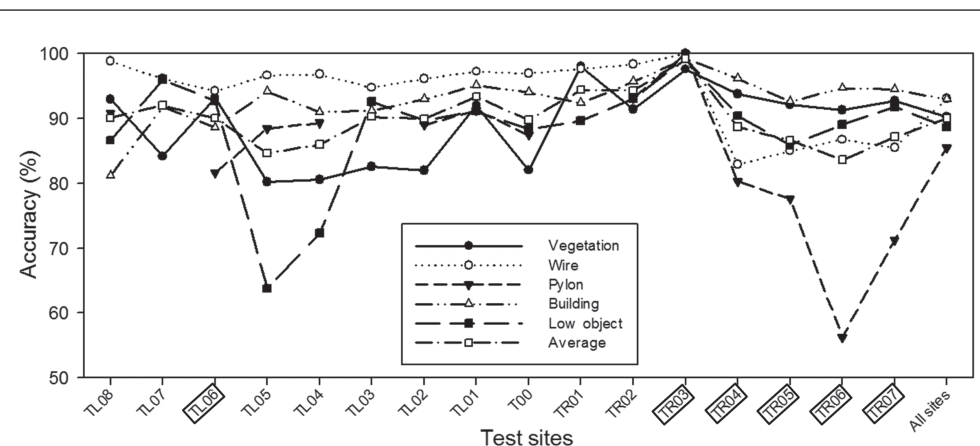


Figure 5. Class-weighted accuracies for each site: Type I sites and Type II sites (black boxed).

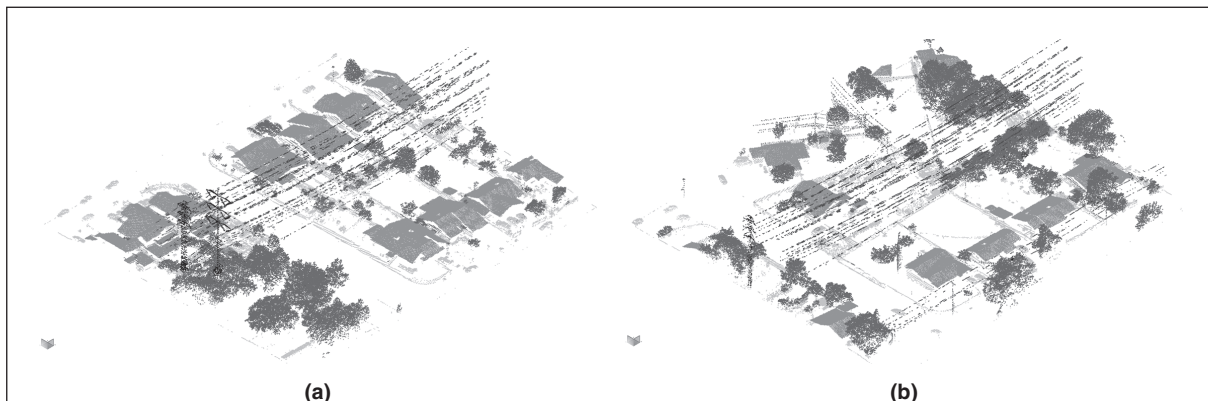


Figure 6. Classification results of Type I site (a) and Type II site, and (b); low object, building, vegetation, wire, and pylon assigned in the order from light to dark gray.

accuracy discrepancy was caused due to a high degree of scene complexity of the test scenes, exhibiting large spatial overlaps between different classes and intra-class variations, which causes complications for the proposed features in differentiating one class from other classes. For instance, we observed that most of the wire class omission errors occurred over regions where the distribution wires pass closely over vegetations. This causes some confusion in vertical-related features to differentiate wire from vegetation or pylon. For pylon objects, most omission errors were observed in small pylons associated with distribution lines, while most commission errors appeared on vegetation, especially over treetops. For vegetation, we discovered that deciduous trees were better classified than coniferous ones. This is due to the fact that coniferous trees are narrow and columnar, so some of them were misclassified into the pylon class. For the building class, we estimated low error rates in both omission and commission. As shown in Table 3, the omission error rate is higher than the commission error rate, and the most omitted building points, especially building wall points, were misclassified into vegetation or low object. Other omission errors locally occurred around building edges where vegetation and buildings are partially overlapped. For the low object class, most of the omission errors were observed from container boxes (in TL05 and TL04), which have been misclassified into buildings because their surface properties are similar to building rooftops. Other misclassification errors occurred at fences located near vegetation, which have been mislabeled as vegetation. In addition, some grasses were misclassified as vegetation.

Thus far, we confirmed that Random Forests trained with proposed features can be considered excellent tools in producing high accurate classification maps for power line risk management. However, we also observed that the elimination of the commission and omission errors produced by the classifier still requires manual editing. Random Forests assigns class labels to raw point of clouds, mainly relying on location information gathered from individual point with its neighboring system. It does not consider certain contextual relations such as spatial arrangement between classes. For instance, one can expect to observe low vegetation underneath power lines with higher probability than other low objects. A Markov Random Field as suggested by Lu *et al.* (2009) would be useful to further eliminate errors produced by Random Forests. Additionally, we found that a leading cause of producing relatively higher classification errors over pylon object is an over-generalization of pylon object class. This problem can be addressed by introducing two separate object classes for distribution and transmission lines. In this study, different features were selected for each class, but their importance was measured for discriminating all the classes, not an individual class from the others. This would require a

future investigation to explore new feature selection methods, especially class-dependent feature selection that can identify which features among entire features distinguish a particular class from the others.

Comparison of Point-based versus Grid-based Feature Extraction

As discussed in the previous section, the classification results shown in Table 3 were produced by Random Forests, which was trained with features that were computed by per-point investigation in 3D. In contrast to this, Guo *et al.* (2011) proposed a grid-based approach where all the points contained in each grid cell were treated as one group, which have the same feature values and thus the same class label.

We have compared the performance of two Random Forests classifiers: point-based (*3D point*) and grid-based (*3D profile*) classifiers. Both classifiers were trained on the same class balanced TR03. To construct a *3D profile* Random Forests, we projected lidar points into a grid space, where each cell size was set to 25 cm by 25 cm. A cylinder (N_c) with its radius of r was created, centered at each grid cell for collecting its neighboring points. To make a fair comparison, we applied the same r value (1.5 m) for both classifiers, with which the same features shown in Table 1 were extracted. Note that the DR feature was excluded in this experiment because it is not applicable for *3D profiles*. Following the same manner used for *3D point* classifiers, we selected the most important feature set for the *3D profiles* of {SP, VE, LN, PE, OS, COS, OD, VD, HG, AN, PD, TE}. These features were reduced to five principle components by PCA. The *3D profiles* trained on the refined feature set classified each grid cell. Then, we assigned the cell's label to all the points within the cell. Finally, we used the labeled points to produce a confusion matrix (Table 4).

Table 4 summarizes classification result over all the test sites produced by *3D profiles*. It was estimated that *3D profiles* produced a sample-weighted accuracy of 86.18 percent and a class-weighted accuracy (an average of accuracies of all the classes) of 84.32 percent. Table 5 describes a confusion matrix of classification produced by *3D profiles* subtracted from that of *3D points*. The positive values of diagonal elements in the matrix indicates that *3D points* have more accurate classification results than *3D profiles*. The negative values of off-diagonal elements indicate that more misclassifications were caused by *3D profiles*. *3D points* resulted in a 4.86 percent and 5.74 percent higher accuracy than *3D profile*, in the sample-weighted and class-weighted accuracies, respectively. We found that *3D points* are superior to *3D profiles* across all the error assessments, with respect to the omission and commission error rate. As can be seen in Table 5, *3D profiles* often produced larger omission and commission errors where multiple classes overlap.

TABLE 4. CONFUSION MATRIX OF 3D PROFILE ($F = 3$, $T = 60$)

Class		Predicted					Omission error (%)
		Vegetation	Wire	Pylon	Building	Low object	
Actual	Vegetation	1,133,569	37,067	2,363	28,570	101,620	13.02
	Wire	8,758	130,309	1,035	520	823	7.87
	Pylon	1,004	3,111	15,020	3	30	21.64
	Building	64,158	6,370	82	969,285	42,075	10.41
	Low object	67,345	11,191	739	39,645	348,654	25.43
Commission error (%)		11.08	30.70	21.93	6.62	29.31	

TABLE 5. SUBTRACTED CONFUSION MATRIX OF 3D PROFILE FROM 3D POINT

		Predicted					Omission error (%)
Class		Vegetation	Wire	Pylon	Building	Low object	
Actual	Vegetation	41,880	-27,863	-192	-11,247	-2,578	-3.21
	Wire	-1,604	1,373	377	305	-451	-0.97
	Pylon	-60	-1,406	1,366	23	77	-7.13
	Building	-27,391	-3,776	-11	36,099	-4,921	-3.34
	Low object	-37,009	-10,853	-689	-17,271	65,822	-14.08
Commission error (%)		-5.07	-21.19	-3.49	-2.75	-4.51	

Computational Time

Our classification approach is composed of two main processing procedures: feature extraction and Random Forests classification. We implemented an algorithm with C++ for the extraction of 21 features and utilized Weka software for Random Forests. The implemented classifier was tested on Windows® 7 with an Intel® Core 2 Quad CPU and 8GB RAM. We estimated the computational times of two classification methods (point-based and grid-based classification), which were previously compared. Consequently, the point-based classifier requires 233 minutes per kilometer for computing the features and classifying the data, while the grid-based classifier took 181 minutes (52 minutes faster). However, the grid-based method misclassified 219,215 points per kilometer, while the point-based misclassified 142,089 points. This suggests that the grid-based method requires additional time to manually re-classify 77,126 misclassified points compared to the point-based classifier. Furthermore, implementing a parallel data processing with multiple computing systems will decrease the importance of the time factor and consequently allow our approach to be applied in a rapid classification of power line scenes.

Conclusions

In this study, we have investigated the potential of a supervised classification method for classifying corridor scenes from airborne lidar data. Random Forests was adopted as a supervised classifier to detect the five key corridor object classes of wire, pylon, building, vegetation, and low objects. We proposed a point-based method, which extracted total 21 features to build Random Forest classifiers. Some feature groups, including the vertical-related feature, were newly designed, particularly for characterizing pylons and wires. The experimental results suggested that it is important to train the classifier with class-balanced training samples. Compared to unbalanced learning, training using balanced data showed 1.33 percent and 4.44 percent higher learning performances in sample-weighted and class-weighted accuracies, respectively. We also realized that balanced learning resulted in an almost equivalent accuracy across all the classes. A sensitivity analysis of classifiers trained with different samples has been conducted. We found that an optimal classification model needs to be trained with a training sample containing more diverse objects representing intra-class variations. The optimal classifier showed high classification results in both sample-weighted (91.04 percent) and class-weighted (90.07 percent) accuracies. The performance of point-based classifier was compared to a grid-based classifier, and the experiments confirmed that the point-based classifier shows 4.86 percent and 5.74 percent higher in the respective sample-weighted and class-weighted accuracy than the grid-based classifier. This outcome suggests that the point-based classifier

is more suitable for the discrimination of vertical overlapping of multiple objects. Even though the proposed supervised classifier has demonstrated its success in corridor scene classification, the classifier still produced misclassification errors that require manual human editing. Thus, further future investigation is necessary to rectify those errors by incorporating contextual information of neighboring classification results, such as adopting Markov Random Field (MRF).

Acknowledgments

This research was supported by a grant "Spatiotemporal Risk Management of Power-line Networks" funded by OCE (Ontario Centre for Excellence), NSERC (Natural Sciences and Engineering Research Council) of Canada, and GeoDigital International, Inc.

References

- Antonarakis, A.S., K.S. Richards, and J. Brasington, 2008. Object-based land cover classification using airborne LiDAR, *Remote Sensing of Environment*, 112(6):2988–2998.
- Breiman, L., 2001. Random forests, *Machine Learning*, 45(1): 5–32.
- Carlberg, M., P. Gao, G. Chen, and A. Zakhari, 2009. Classifying urban landscape in aerial LiDAR using 3D shape analysis, *Proceeding of Image Processing (ICIP), 2009, 16th IEEE International Conference*, 07–10 November, pp. 1701–1704.
- Chawla, N.V., K.W. Bowyer, L.O. Hall, and W.P. Kegelmeyer, 2002. Smote: Synthetic minority oversampling technique, *Journal of Artificial Intelligence Research*, 16:321–357.
- Chehata, N., L. Guo, and C. Mallet, 2009. Airborne LiDAR feature selection for urban classification using Random Forests, *Proceeding of Laser scanning 2009, IAPRS, Vol. XXXVIII, Part 3/W8, 01–02 September, Paris, France*, pp. 207–212.
- Chen, C., A. Liaw, and L. Breiman, 2004. *Using Random Forests to Learn Imbalanced Data*, Technical Report, Department of Statistics, University of California.
- Coulston, J.W., G.G. Mosen, B.T. Wilson, M.V. Flinco, W.B. Cohen, and C.K. Brewer, 2012. Modeling percent tree canopy cover: A pilot study, *Photogrammetric Engineering & Remote Sensing*, 78(7):715–727.
- Flood, M., 2011. Workflow challenges on airborne lidar electrical transmission projects, *Photogrammetric Engineering & Remote Sensing*, 77(5):438–443.
- Forlani G., C. Nardinocchi, M. Scaioni, and P. Zingaretti, 2006. Complete classification of raw LIDAR data and 3D reconstruction of building, *Pattern Analysis and Applications*, 8(4):357–374.
- Guo, L., N. Chehata, C. Mallet, and S. Boukir, 2011. Relevance of airborne lidar and multispectral image data for urban scene classification using Random Forests, *ISPRS Journal of Photogrammetry and Remote Sensing*, 66(1):56–66.
- Guo, Q., W. Li, D. Liu, and J. Chen, 2012. A framework for supervised image classification with incomplete training samples, *Photogrammetric Engineering & Remote Sensing*, 78(6):595–604.

- Hough, P., 1962: *Method and Means for Recognizing Complex Patterns*, U.S. Patent 3.069.654.
- Ituen, I., and G. Sohn, 2010. The way forward: Advances in maintaining right-of-way of transmission lines, *GEOMATICA*, 64(40):451–462.
- Jwa, Y., and G. Sohn. 2012. A piecewise catenary curve model growing for 3D power line reconstruction, *Photogrammetric Engineering & Remote Sensing*, 78(12):1227–1240.
- Kim, E., and G. Medioni, 2011. Urban Scene Understanding from aerial and ground LIDAR data, *Machine Vision and Applications (MVA)*, 22(4):691–703.
- Lalonde, J., N. Vandapel, D. Huber and M. Hebert, 2006. Natural terrain classification using three-dimensional ladar data for ground robot mobility, *Journal of Field Robotics*, 23(10):839–861.
- Lehtomäki, M., A. Jaakkola, J. Hyppä, A. Kukko, and H. Kaartinen, 2010. Detection of vertical pole-like objects in a road environment using vehicle-based laser scanning data, *Remote Sensing*, 2(3):641–664.
- Liang, J., J. Zhang, K. Deng, Z. Liu, and Q. Zhi, 2011. A new power-line extraction method based on airborne LiDAR point cloud data, *International Symposium on Image and Data Fusion*, 09–11 August, pp. 1–4.
- Lim, E.H., and D. Suter, 2009. 3D terrestrial lidar classifications with super-voxels and multi-scale conditional random fields, *Computer-Aided Design*, 41(10):701–710.
- Lin, C., G. Thomson, C.S. Lo, and M.S. Yang, 2011. A multi-level morphological active contour algorithm for delineating tree crowns in mountainous forest, *Photogrammetric Engineering & Remote Sensing*, 77(3):241–249.
- Lodha, S.K., D. Fitzpatrick and D.P. Helmbold, 2007. Aerial lidar data classification using expectation-maximization, *Proceedings of SPIE Conference on Vision Geometry*, XIV, Volume 6499.
- Lu, W.L., K.P. Murphy, J.J. Little, A. Sheffer, and H. Fu, 2009. A hybrid conditional random field for estimating the underlying ground surface from airborne LiDAR data, *IEEE Geoscience and Remote Sensing*, 47(82):2913–2922.
- McLaughlin, R.A., 2006. Extracting transmission lines from airborne LiDAR data, *IEEE Geoscience and Remote Sensing Letters*, April, 3(2):222–226.
- Melzer, T., and C. Briese, 2004. Extraction and modeling of power lines from ALS point clouds, *Proceedings of 28th Workshop of the Austrian Association for Pattern Recognition*, pp. 47–54.
- Na, X., S. Zhang, X. Li, H. Yu, and C. Liu, 2010. Improved land cover mapping using Random Forests combined with Landsat Thematic Mapper imagery and ancillary geographic data, *Photogrammetric Engineering & Remote Sensing*, 76(7):833–840.
- Neuenschwander, A.L., L.A. Magruder, and M. Tyler, 2009. Landcover classification of small-footprint, full-waveform lidar data, *Journal of Applied Remote Sensing*, 3(1):033544–033544.
- Niemeyer, J., J.D. Wegner, C. Mallet, F. Rottensteiner and U. Soergel, 2011. Conditional random fields for urban scene classification with full waveform LiDAR data, *Photogrammetric Image Analysis (PIA)* U. Stilla, F. Rottensteiner, H. Mayer, B. Jutzi, and M. Butenuth, editors), LNCS 6952, Springer, Heidelberg, pp. 233–244.
- Rabbani, T., and F. van den Heuvel, 2005. Efficient Hough Transform for automatic detection of cylinders in point clouds, *International Archives of Photogrammetry, Remote Sensing and Spatial Information Sciences*, XXXVI-3/W19, pp. 60–65.
- Rodriguez-Galiano, V.F., B. Ghimire, E. Pardo-Iguzquiza, M. Chica-Olmo, and R.G. Congalton, 2012. Incorporating the downsampled Landsat TM thermal band in land-cover classification using Random Forest, *Photogrammetric Engineering & Remote Sensing*, 78(2):129–137.
- Rutzinger, M., B. Höfle, M. Hollaus, and N. Pfeifer, 2008. Object-based point cloud analysis of full-waveform airborne laser scanning data for urban vegetation classification, *Sensors*, 8(8):4505–4528.
- Samadzadegan, F., H. Hasani, and T. Schenk, 2012. Determination of optimum classifier and feature subset in hyperspectral images based on ant colony system, *Photogrammetric Engineering & Remote Sensing*, 78(12):1261–1273.
- Sohn, G., and I. Dowman, 2008. A model-based approach for reconstructing terrain surface from airborne LiDAR data, *The Photogrammetric Record*, 23(122):170–193.
- Sutton, C.D., 2005. Classification and regression trees, bagging, and boosting, *Handbook of Statistics: Data Mining and Data Visualization* (C. R.Rao, E.J. Wegman, and J.L. Solka, editors), Elsevier Publishing, Amsterdam, The Netherlands, Vol. 24, pp. 303–329.
- Verma, V., R. Kumar, and S. Hsu, 2006. 3D building detection and modeling from aerial lidar data, *Proceedings of the IEEE Conference on Computer Vision and Pattern Recognition*, October, pp. 2213–2220.
- Waske, B., and M. Braun, 2009. Classifier ensembles for land cover mapping using multitemporal SAR imagery, *ISPRS Journal of Photogrammetry and Remote Sensing*, 64(5):450–457.
- Yu, X., J. Hyppä, M. Holopainen, M. Vastaranta, and R. Viitala, 2011. Predicting individual tree attributes from airborne laser point clouds based on Random Forests technique, *ISPRS Journal of Photogrammetry and Remote Sensing*, 66(1):28–37.
- Zhang, J., and G. Sohn, 2010. A Markov Random Field Model for individual tree detection from airborne laser scanning data, *Proceedings of Photogrammetric Computer Vision (PCV) 2010*, 01–03 September, Paris, France, *International Archives of Photogrammetry and Remote Sensing*, 38(3A):120–125.

(Received 29 October 2012; accepted 21 January 2013; final version 15 April 2013)